



# Multigenerational memory and adaptive adhesion in early bacterial biofilm communities

Calvin K. Lee<sup>a,b,c,1</sup>, Jaime de Anda<sup>a,b,c,1</sup>, Amy E. Baker<sup>d</sup>, Rachel R. Bennett<sup>e,f</sup>, Yun Luo<sup>d,g</sup>, Ernest Y. Lee<sup>a,b,c</sup>, Joshua A. Keefe<sup>a,b,c</sup>, Joshua S. Helali<sup>a,b,c</sup>, Jie Ma<sup>a,b,c</sup>, Kun Zhao<sup>h,i,2</sup>, Ramin Golestanian<sup>e,2</sup>, George A. O'Toole<sup>d,2</sup>, and Gerard C. L. Wong<sup>a,b,c,2</sup>

<sup>a</sup>Department of Bioengineering, University of California Los Angeles, CA 90095; <sup>b</sup>Department of Chemistry and Biochemistry, University of California Los Angeles, CA 90095; <sup>c</sup>California NanoSystems Institute, University of California Los Angeles, CA 90095; <sup>d</sup>Department of Microbiology and Immunology, Geisel School of Medicine at Dartmouth, Hanover, NH 03755; <sup>e</sup>Rudolf Peierls Centre for Theoretical Physics, University of Oxford, OX1 3NP Oxford, United Kingdom; <sup>f</sup>Department of Physics, University of Pennsylvania, Philadelphia, PA 19104; <sup>g</sup>DuPont Industrial Bioscience, Palo Alto, CA 94304; <sup>h</sup>Key Laboratory of Systems Bioengineering (Ministry of Education), School of Chemical Engineering and Technology, Tianjin University, Tianjin 300072, People's Republic of China; and <sup>i</sup>SynBio Research Platform, Collaborative Innovation Center of Chemical Science and Engineering (Tianjin), Tianjin University, Tianjin 300072, People's Republic of China

Edited by Caroline S. Harwood, University of Washington, Seattle, WA, and approved February 27, 2018 (received for review November 30, 2017)

Using multigenerational, single-cell tracking we explore the earliest events of biofilm formation by *Pseudomonas aeruginosa*. During initial stages of surface engagement (<20 h), the surface cell population of this microbe comprises overwhelmingly cells that attach poorly (~95% stay <30 s, well below the ~1-h division time) with little increase in surface population. If we harvest cells previously exposed to a surface and direct them to a virgin surface, we find that these surface-exposed cells and their descendants attach strongly and then rapidly increase the surface cell population. This “adaptive,” time-delayed adhesion requires determinants we showed previously are critical for surface sensing: type IV pili (TFP) and cAMP signaling via the Pil-Chp-TFP system. We show that these surface-adapted cells exhibit damped, coupled out-of-phase oscillations of intracellular cAMP levels and associated TFP activity that persist for multiple generations, whereas surface-naïve cells show uncorrelated cAMP and TFP activity. These correlated cAMP-TFP oscillations, which effectively impart intergenerational memory to cells in a lineage, can be understood in terms of a Turing stochastic model based on the Pil-Chp-TFP framework. Importantly, these cAMP-TFP oscillations create a state characterized by a suppression of TFP motility coordinated across entire lineages and lead to a drastic increase in the number of surface-associated cells with near-zero translational motion. The appearance of this surface-adapted state, which can serve to define the historical classification of “irreversibly attached” cells, correlates with family tree architectures that facilitate exponential increases in surface cell populations necessary for biofilm formation.

bacteria biofilms | *Pseudomonas aeruginosa* | surface sensing | type IV pili | cyclic AMP

Recent work has shown that bacteria can orchestrate community-scale behavior between neighboring cells, such as alternating the growth of the biofilm interior and that of the periphery via electrochemical signals (1–3), or coordinate biofilm organization via quorum sensing (4–6). Can bacteria orchestrate similar communication between ancestor and descendant cells? Since cells in the same lineage are temporal neighbors rather than spatial neighbors, this mode of signaling can be mediated by intracellular rather than extracellular molecules. We examine *Pseudomonas aeruginosa* PA14 as a model system for this type of familial communication in the context of surface sensing, the first step in the formation of biofilm communities from planktonic cells (7). A brief review is included in *SI Discussion*. Recent work on *P. aeruginosa* PA14 has shown that type IV pili (TFP) are a key sensor component for first contact, followed by cAMP up-regulation (8–11). Increased cAMP levels in turn stimulate TFP biogenesis and activity via the Pil-Chp system, initiating a cascade that ultimately activates c-di-GMP signaling (8). Rising c-di-GMP levels in turn promote flagellar shutdown and exopolysaccharide (EPS) matrix production (8, 9), key

steps in establishing a biofilm. Here, we engage the canonical problem that all biofilm-forming bacteria face: how they sense and adaptively adhere to abiotic surfaces. Single-cell tracking methods are combined with analysis of TFP activity and single-cell measurements of cAMP. We show that surface sensing signals can be propagated as a type of memory across multiple bacterial generations via damped coupled oscillations of cAMP levels and TFP activity, resulting eventually in a drastic suppression of TFP motility and the rise of family tree architectures that exponentially increase bacterial populations on a surface.

## Results

**“Surface-Naïve” and “Surface-Sentient” Planktonic Bacteria Exhibit Different Surface Population Behaviors.** We examine the difference between “surface-sentient” cells that have previously landed on the surface and “surface-naïve” cells that have never been exposed

## Significance

Bacteria use multigenerational memory based on coupled oscillations of cAMP levels and type IV pili (TFP) activity to adaptively adhere to surfaces. These oscillations create cells with a “surface-sentient” state intermediate between planktonic and sessile, characterized by coordinated surface motility suppression. This intermediate state drastically increases the number of surface nonmotile cells and correlates with a transition in family tree architectures toward exponential surface population growth. Our data support the idea that reversible attachment is vital for irreversible attachment. That is, repeated sensing, division, and detachment cycles create a planktonic population with robust cAMP-TFP-based memory of the surface, allowing cells to return to the surface progressively better adapted for sensing and attachment, ultimately dominating the surface ecology via exponential surface population increase.

Author contributions: C.K.L., J.d.A., K.Z., R.G., G.A.O., and G.C.L.W. designed research; C.K.L., J.d.A., A.E.B., J.A.K., J.S.H., and K.Z. performed research; C.K.L., J.d.A., A.E.B., R.R.B., Y.L., E.Y.L., K.Z., R.G., G.A.O., and G.C.L.W. contributed new reagents/analytic tools; C.K.L., J.d.A., A.E.B., R.R.B., J.A.K., J.S.H., J.M., K.Z., and R.G. analyzed data; and C.K.L., J.d.A., A.E.B., R.G., G.A.O., and G.C.L.W. wrote the paper.

The authors declare no conflict of interest.

This article is a PNAS Direct Submission.

Published under the PNAS license.

Data deposition: Binary images and the fluorescence images have been deposited on Figshare, <https://doi.org/10.6084/m9.figshare.5969335>.

<sup>1</sup>C.K.L. and J.d.A. contributed equally to this work.

<sup>2</sup>To whom correspondence may be addressed. Email: kunzhao@tju.edu.cn, ramin.golestanian@physics.ox.ac.uk, georgeo@dartmouth.edu, or gclwong@seas.ucla.edu.

This article contains supporting information online at [www.pnas.org/lookup/suppl/doi:10.1073/pnas.1720071115/-DCSupplemental](http://www.pnas.org/lookup/suppl/doi:10.1073/pnas.1720071115/-DCSupplemental).

to the surface. Since the planktonic population in a flow cell inherently comprises both surface-naïve and surface-sentient subpopulations, we connect two flow cells (FC1 and FC2) in series (*SI Materials and Methods*) to investigate how the planktonic population changes as it engages the surface. Analysis of family trees is used as a tool to monitor cell fate: whether each surface-engaged cell stays on the surface and whether subsequent daughter cells remain on the surface or return to the planktonic population. We monitor the intracellular cAMP levels for each WT cell using a cAMP-responsive reporter plasmid at different time points (Fig. 1). The *P. aeruginosa*-borne reporter strain produces YFP in response to cAMP changes, which is normalized by constitutive CFP expression (*SI Materials and Methods*).

Immediately after initial inoculation of FC1 (defined as  $t_1 = 0$ ) with planktonic, surface-naïve cells and for the next  $\sim 20$  h, the observed surface bacterial population is composed overwhelmingly of cells with low cAMP (Fig. 1A) and cells that attach transiently, with  $\sim 95\%$  of cells (1,365 bacteria measured) staying only 3–30 s (Fig. 1B), not enough for a division cycle on the surface ( $\sim 1$  h, Fig. S1). These early cells exhibit low levels of normalized cAMP reporter intensities of  $I_{cAMP} \sim 1.55 \pm 0.21$  (median  $\pm$  median absolute deviation) during the first hour after inoculation (Fig. 1A, Top Left and Fig. S2, Top). For  $t_1 < 20$  h ( $t_n$  = time in FC $n$ ), the number of observed fluorescent reporter cells on the surface is small (Fig. 1A), consistent with the fact that most cells have dwell times that are much shorter than 15 min (the time between fluorescence measurements). After the initial  $\sim 4$  h, the surface residence times of cells begin to increase (Fig. S2). However, due to the large numbers of detached cells, the total surface cell population does not increase. At  $t_1 \sim 22$  h, the total number of surface bacteria begins to increase markedly, and we no longer observe consecutive empty frames without bacteria (Fig. 2B, Top). Between  $t_1 \sim 22$ –29.5 h (end of run in FC1), in addition to a population with low  $I_{cAMP}$ , a population of surface-engaged cells with increased cAMP ( $I_{cAMP} \sim 3$ –6) emerges (Fig. 1A, Top Right). Of all of the 1,450 cells that we analyzed for family structure in the full history of FC1 (29.5 h), we find that  $\sim 95\%$  consist of single-generation bacteria (Fig. 2C, Top).

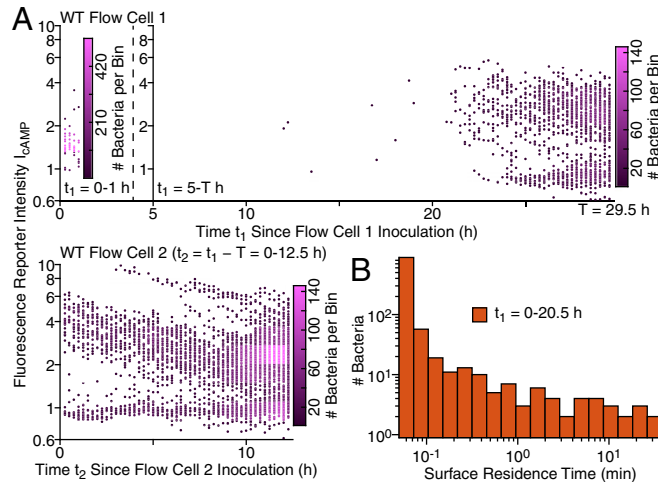


**Fig. 1.** Surface-naïve and surface-sentient planktonic bacteria exhibit drastically different behavior on the surface. (A) Fluorescence reporter intensities ( $I_{cAMP}$ ) for WT in FC1 (Top) and FC2 (Bottom) vs. time since first exposure to bacteria ( $t_n = 0$ ). T = 29.5 h represents the time when bacteria in FC1 are harvested and introduced to virgin FC2. Data points are colored by the total number of cells per heat-map bin. For clarity, overlapping points are omitted. The top left, top right, and bottom heat maps are generated from 2,104, 1,441, and 3,935 bacterium measurements every 30 s, 15 min, and 15 min, respectively. (B) Histograms of surface residence times for the tracked cells during  $t_1 = 0$ –20.5 h (1,365 bacteria tracked using the bright-field images), using logarithmic binning (19 logarithmically spaced bin edges between 3 s and 38 min) and plotted on log-log axes.

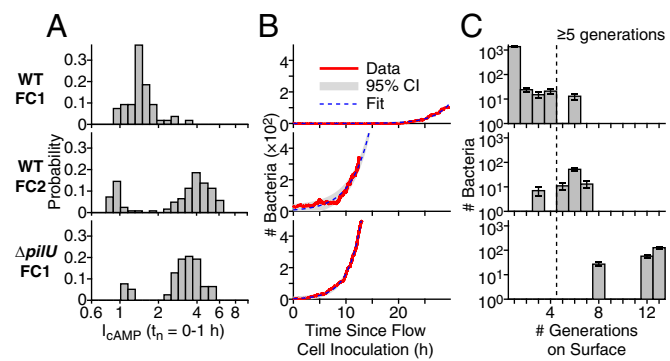


**Fig. 2.** WT FC2 is different from WT FC1 but like the  $\Delta p i l U$  mutant in FC1. (A) Histograms of normalized cAMP reporter intensities ( $I_{cAMP}$ ) ( $t_n = 0$ –1 h) using logarithmically spaced bins. Histograms are generated from  $n = 54$ , 124, and 78 measurements of bacteria in four fluorescence frames (every 15 min) for WT FC1 (T = 29.5 h), WT FC2 (T = 29.5 h), and the  $\Delta p i l U$  mutant in FC1. WT FC1 has a single peak centered around  $I_{cAMP} \sim 1.5$ . WT FC2 and  $\Delta p i l U$  FC1 have two peaks centered around  $I_{cAMP} \sim 1$  and 4. (B) The number of surface bacteria per frame vs. time remains near zero for  $\sim 20$  h, and increases slowly for WT FC1 (Top) but increases immediately and much faster for WT FC2 (Middle) and  $\Delta p i l U$  FC1 (Bottom). Solid lines represent data. Dashed lines represent data fit to exponential functions. Shaded areas represent 95% CI of the fits. (C) Distribution of the total number of surface generations of the family each bacterium is part of for the same data in B. Error bars indicate relative error of  $1/\sqrt{n}$  of no. of points per bin. Bacteria in families with at least five generations are relatively rare for WT FC1 (Top) but are much more common for WT FC2 (Middle) and  $\Delta p i l U$  FC1 (Bottom) (vertical dashed line).

Interestingly, during the emergence of the population with increased cAMP near the end of the run of FC1 ( $t_1 \sim 22$ –29.5 h), bacteria that are part of families with more generations are observed, with the largest families at six generations (Fig. 2C, Top). These results in Figs. 1 and 2 show that a subpopulation of cells that attach during the last approximately one-third of the FC1 experiment behaves drastically differently than cells that attach during the first approximately two-thirds of the experiment.

To assess the behavior of planktonic populations composed of surface-sentient cells that have had the opportunity to engage a surface, a two-flow-cell array in series was used to harvest the mixture of surface-naïve and surface-sentient planktonic cells from FC1 at a specific surface cell density level (corresponding to a time point T = 29.5 h after  $t_1 = 0$ ) (Fig. 1A, Top) and track their behavior in virgin FC2 (Fig. 1A, Bottom), which has not had previous exposure to bacterial attachment or potential bacterial factors that condition the surface for adhesion (e.g., EPS, proteins, or DNA). To facilitate comparison with FC1, we reset time to  $t_2 = t_1 - T$  in FC2, so that  $t_2 = 0$  corresponds to inoculation of FC2. If surface-naïve and surface-sentient cell behave similarly, then we expect little surface population growth for  $\sim 20$  h, as in FC1. Contrary to this null hypothesis, a sizable population of cells attach immediately ( $t_2 = 0$  h) in FC2 and subsequently exhibits a sharp increase in population after  $t_2 \sim 8$  h (Fig. 2B, Middle).

By comparing and fitting the curves in Fig. 2B to exponential functions ( $N(t_n) = N(0)\exp((t_n - t_{lag})/\tau)$ ), where  $N(t_n)$  is the number of bacteria in FC $n$  at time  $t_n$ ,  $t_{lag}$  is the time lag before exponential growth begins, and  $\tau$  is the time constant for the observed exponential growth, the surface population growth in FC1 and FC2 is found to be significantly different:  $t_{lag} = 17.56$  h (mean) [17.53 h, 17.59 h] (95% confidence interval) for WT FC1 vs. 4.68 h [4.65 h, 4.72 h] for WT FC2. We note that even varying parameters in an exponential fit does not fully capture the stark deviation of behavior in FC2, indicated by the nonzero baseline and wider 95% confidence interval of the fit for  $t_2 < 5$  h. Of the bacteria that we analyzed in family trees in FC2, most attached cells are part of multigenerational families rather than a single generation as in FC1 (Fig. 2C, Top and Middle and Fig. S3). Comparing the distributions between FC1 and FC2 in

Fig. 2C using a Kruskal–Wallis test yields a  $P$  value  $\ll 10^{-5}$ , indicating that these populations are significantly different.

Repeats of tandem flow cell experiments at different time points yield mutually consistent results. When the total available duration of bacterial surface exposure is reduced by harvesting planktonic bacteria at a lower surface cell density ( $T = 26.75$  h), then the bacterial surface population growth in WT FC2 is retarded by  $\sim 8$  h (Fig. S4A, Top and Middle). A repeat of these experiments with three tandem flow cells shows that FC2 and FC3 have similarly fast rates of surface population growth compared with FC1, while FC1 has no detectable surface population growth for  $\sim 25$  h (Fig. S4B); these data suggest that cells in FC2 have already saturated their level of surface sentience and are thereby surface-adapted.

### Mutants Altered in cAMP Signaling Exhibit Key Differences in Family Tree Architecture.

If there were no differences between surface-naïve and surface-sentient cells, then we would expect cAMP levels of attached cells in FC2 to mirror those of FC1. What we observe is quite different. Cells that initially attach in FC2 have higher cAMP levels ( $I_{cAMP} \sim 4$ ) (Fig. 2A, Middle) than those that initially attach in FC1 ( $I_{cAMP} \sim 1.5$ ) (Fig. 2A, Top). These data indicate that cAMP levels increase for cells that have previously engaged the surface.

An independent way to assay the impact of cAMP levels on surface population increase is by using mutants altered in cAMP signaling. Since the  $\Delta pilU$  mutant is known to have higher baseline cAMP levels (8, 12, 13), we hypothesize that planktonic cells of the  $\Delta pilU$  mutant should behave like cells that have been surface-engaged. The  $\Delta pilU$  mutant cells in FC1 show systematically higher average levels of cAMP during the first hour of surface engagement ( $I_{cAMP} \sim 4$ ) (Fig. 2A, Bottom) compared with WT in FC1 ( $I_{cAMP} \sim 1.5$ ) (Fig. 2A, Top). In agreement with our hypothesis, behavior of the  $\Delta pilU$  mutant in FC1 is similar to the behavior of WT in FC2. That is, the  $\Delta pilU$  mutant exhibits similar or faster rates of surface population growth compared with that for WT in FC2 ( $t_{lag} = -0.35$  h [ $-0.36$  h,  $-0.34$  h] in Fig. 2B, Bottom and  $t_{lag} = -0.32$  h [ $-0.35$  h,  $-0.30$  h] in Fig. S4A, Bottom), with more cells in larger family trees as for the WT in FC2 (Fig. 2C, Bottom).

We analyzed family tree architecture and cAMP levels for WT and other mutants that impact cAMP levels. Most cells in FC1 are transiently engaged with the surface with few cells or their progeny remaining on the surface for  $>30$  s, thus resulting in little or no net growth in the surface population and low median cAMP levels (Figs. 1 and 2). In FC2, we observed that more cells and their subsequent progeny remained on the surface and the median cAMP level increases. To compare the behavior of WT to mutants altered in cAMP signaling, we used multi-generational cell-tracking methods (Fig. 3). We quantified family trees using two metrics. The first metric is used to characterize each division event in a tree, which can be one of three types of division branching. “Two-legged” branching occurs when both daughter cells remain surface-attached, “one-legged” when one daughter cell detaches, and “zero-legged” when both daughter cells detach. The second metric is used to characterize the architecture of entire family trees. We calculate a “tree asymmetry” parameter  $\lambda$  so that  $\lambda = 0$  corresponds to ideal trees with purely two-legged division branching and  $\lambda = 1$  to ideal trees with purely one-legged division branching (SI Materials and Methods). WT trees are clearly heterogeneous, which is expected for signal transduction systems where noise and fluctuations are important. However, for the first six generations of surface engagement, WT trees tend to have more one-legged division branching ( $\lambda_6 = 0.76 \pm 0.10$ , mean  $\pm$  SD).

Given the link between TFP activity and intracellular cAMP levels (8, 9, 13), we tracked family trees for pilin mutants with different cAMP levels (Fig. 3 and Fig. S5). The  $\Delta pilA$  mutant, which has no TFP and low cAMP (14), exhibits predominantly one-legged branching. Similar behavior is observed for the  $\Delta pilT$  mutant, which has intact TFP but is not able to retract them (15), and for  $\Delta pilJ$ , the deletion mutant for the sensory protein component of the Pil-Chp system (16). Moreover, these mutants all

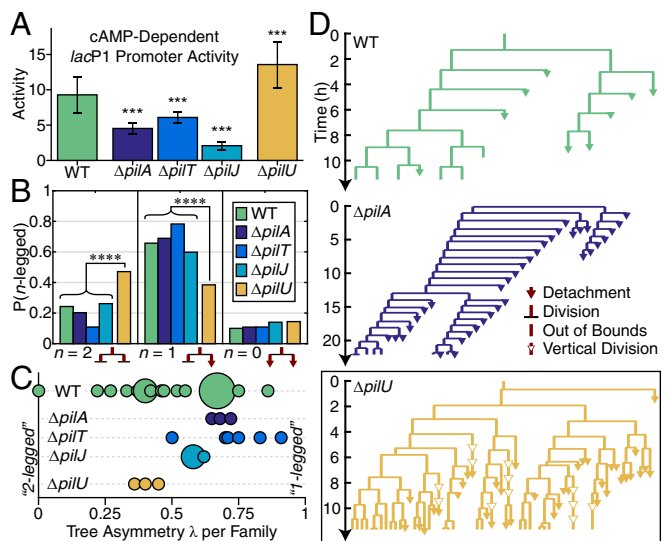


**Fig. 3.** WT and surface-sensing mutants exhibit key differences in family tree architecture. (A) cAMP-dependent *lacP1-lacZ* promoter activity is represented as fold change of *lacP1-lacZ* promoter activity over a vector control. Values are reported as mean  $\pm$  SD from three independent experiments with three replicates each. (\*\* $P < 0.001$  compared with WT.) (B) Proportions of “n-legged” division branching per strain, where  $n$  is the number of non-detached daughter cells postdivision. Data represent 70~110 events per strain.  $\chi^2$  tests are performed to determine statistical differences in the observed proportions.  $n = 2$  and  $n = 1$  had  $\chi^2$  test  $P$  values of  $1.19 \times 10^{-5}$  and  $6.03 \times 10^{-6}$ , respectively, indicating that there are statistical differences among the strains. Further pairwise  $\chi^2$  tests and the Benjamini and Yekutieli (17) procedure for controlling the false discovery rate of a family of hypothesis tests show that the  $\Delta pilU$  mutant is significantly different from the other strains (\*\*\*\* $P < 10^{-4}$ ). If postdivision outcomes were randomly distributed, then the probabilities for  $n=0,1,2$  would be  $q^2, 2q(1-q), (1-q)^2$ , respectively, where  $q$  is any number between 0 and 1. There is no way to reproduce observed distributions in the figure for any value of  $q$ , so correlations must exist in the system. (C) Tree asymmetry  $\lambda$  characterizes a family's overall division branching behavior. Circle area is proportional to the number of families with the same  $\lambda$  (three or more families per strain,  $\geq 10$  bacteria per family). (D) Family trees for WT and TFP-related gene deletion mutants. A small fraction of  $\Delta pilU$  cells divide while vertical (open triangles), similar to *Caulobacter crescentus* (27).

exhibit significantly lower cAMP than the WT (Fig. 3A) and take much longer to form biofilms in our experiments. Fig. 3B shows that, for  $t_1 < \sim 25$  h, WT,  $\Delta pilA$ ,  $\Delta pilT$ , and  $\Delta pilJ$  all qualitatively exhibit preponderance of one-legged branching (~60–80% vs. ~40% for  $\Delta pilU$ ), which does not contribute to surface population growth. In contrast, the  $\Delta pilU$  mutant, which has increased cAMP levels (Fig. 3A), shows a much greater proportion of two-legged branching (~50% vs. ~10–25% for the other four strains) and does so almost immediately after surface contact of the progenitor cell that starts the family. Pairwise  $\chi^2$  tests and Benjamini and Yekutieli (17) procedure for controlling the false discovery rate of a family of hypothesis tests show that  $\Delta pilU$  is significantly different from the other strains with a  $P$  value  $< 10^{-4}$ . If we measure the statistics of division-branching events during just the first six generations (Fig. S6), the patterns remain similar. The  $\Delta pilU$  mutant exhibits a higher proportion of two-legged branching (~50%) compared with the other four strains (~15–25%) and a lower proportion of one-legged branching (~30% vs. ~60–70% for the other four strains).

If entire family trees are compared statistically for all mutants (Fig. 3 C and D and Fig. S7), informative behavioral patterns emerge:  $\Delta pilA$ ,  $\Delta pilT$ , and  $\Delta pilJ$  trees, although heterogeneous, tend to be clustered near one-legged values of  $\lambda$  ( $0.68 \pm 0.03$ ,  $0.73 \pm 0.14$ , and  $0.60 \pm 0.02$  for  $\Delta pilA$ ,  $\Delta pilT$ , and  $\Delta pilJ$ , respectively) and  $\Delta pilU$  near two-legged values of  $\lambda$  ( $0.40 \pm 0.05$ ).

with statistically significant differences between them (e.g.,  $\Delta pilA$  is significantly different from  $\Delta pilU$  with a  $P$  value of 0.045 and  $\Delta pilT$  from  $\Delta pilU$  with a  $P$  value of 0.008). It is telling that WT is capable of eventually generating heterogeneous trees that range over the entire spectrum, from one-legged to two-legged ( $\lambda = 0.47 \pm 0.21$ , with  $\lambda$  ranging between 0–0.86), even though its early trees tend to be one-legged (for first six generations,  $\lambda_6 = 0.76 \pm 0.10$ ). The evolution of division branching in family trees is a stochastic rather than a monotonic process. A structural characteristic of these stochastic processes is the inherently large number fluctuations in the system, which can lead to a larger data spread than standard Poissonian fluctuations. However, these data strongly suggest that a key downstream consequence of TFP-cAMP-based surface sensing is the transition from one-legged to two-legged division branching, which is in fact mathematically required for the observed transition from sublinear growth to exponential growth in the surface population of cells and constitutes a pivotal event in biofilm development.

**Coupled Oscillations of cAMP and TFP Activity Propagate Across Multiple Generations in Family Lineages of Surface Bacteria.** Given that cAMP levels varied with the attachment behavior, enhancing cAMP levels by mutation (i.e., the  $\Delta pilU$  mutant), and our reported link between surface-specific cAMP up-regulation and TFP, we predicted that this secondary messenger and TFP activity have a complex temporal relation to one another. To see this, we built a stochastic model that describes cAMP, TFP, and the cAMP signaling system (called Pil-Chp) (8, 9) and quantitatively compare the model with measured data for entire lineages of cells, so that we can better understand how cAMP and TFP activity are coordinated during early events in surface engagement within this conceptual framework. Intracellular levels of cAMP for individual cells are measured using the plasmid reporter above. TFP-driven motility, known as “twitching” motility, is characterized by directional motion with jittery changes of direction. Based on our previous work on quantifying twitching activity in WT and flagellum deletion mutants, we designed a multimetric algorithm to recognize diverse forms of TFP activity without human bias, by measuring a cell’s mean squared displacement (18), radius of gyration (19), and visit map (20) over time scales from seconds to minutes (21) and comparing results to known characteristics of twitching from our previous reference measurements (details are given in *SI Materials and Methods* and Fig. S8).

The basic ingredients of the model (Fig. 4A) are the time-dependent concentrations of PilA monomer  $m(t)$ , cAMP signal  $s(t)$ , and TFP activity  $A(t)$  (*SI Materials and Methods*). The dynamical equations relating these quantities are nonlinear and coupled, but the system’s responses and fluctuations can be calculated using a phenomenological method that follows the spirit of Turing’s seminal work on generic reaction-diffusion systems (22). To understand the complex temporal relationship between cAMP and TFP, we compare experimental data with this model. As in all studies of bacterial intracellular signaling, weak features are difficult to pick out from raw data when they coexist with noise and reside on top of strong average trends (Fig. S9). Here we employ standard signal processing techniques to circumvent these problems. To find and isolate the weak periodic signals predicted by theory, we plot in Fig. 4B for WT FC2 ( $T = 29.5$  h) the time-dependent autocorrelation function of TFP activity (*Left*), the autocorrelation function of cAMP signal (*Center*), and the cross-correlation function between cAMP and TFP activity (*Right*) and show that they can be fit to predictions of the model with good fidelity.

Since cAMP correlates with piliation, it is tempting to assume that high levels of cAMP will be correlated to high levels of TFP activity. Both the experimental data and the model show otherwise. The peak at  $\sim 5$  h in the cross-correlation function between cAMP and TFP activity (Fig. 4B, *Right*) indicates that high levels of cAMP are correlated with high levels of TFP at a time lag  $\sim 5$  h later. That is, maximal TFP activity occurs  $\sim 5$  h after

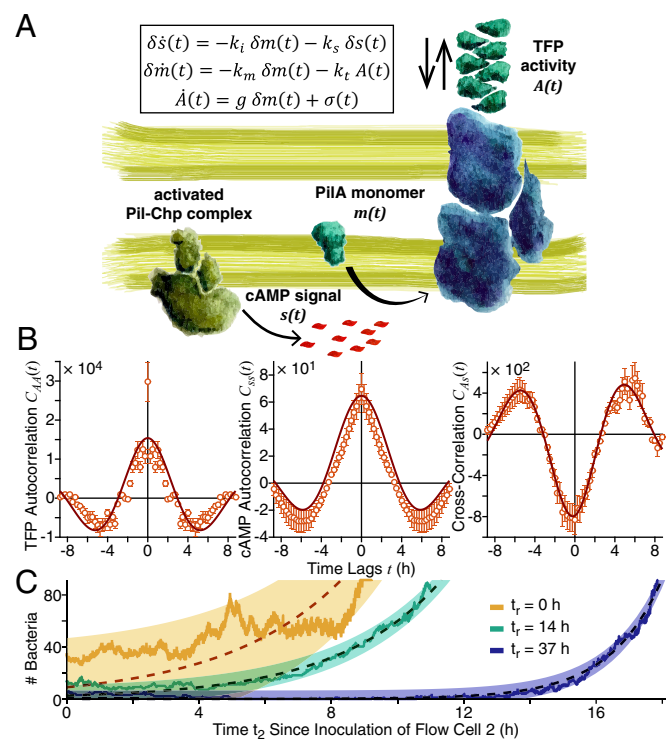


**Fig. 4.** Multigenerational cAMP-TFP signal transduction drives memory and memory loss. (A) Schematic of the stochastic model that describes multigenerational cAMP-TFP signal transduction, illustrating the model components [PilA monomer  $m(t)$ , cAMP signal  $s(t)$ , and TFP activity  $A(t)$ ]. (Inset) The equations relating these components. (B) Comparison of model and experiments using the correlation functions  $C_{AA}(t)$  (*Left*),  $C_{ss}(t)$  (*Middle*), and  $C_{As}(t)$  (*Right*) calculated from data for one family in WT FC2. Circles are experimental data. Error bars indicate relative error of  $1/\sqrt{\text{no. of points per time lag}}$ . Solid lines indicate the model fit (parameters:  $[k, \omega_0, k_s, D, k_t] = [0.12, 0.6, -0.35, 3200, 0.025]$ ). There are negative and positive cross-correlations (*Right*) at time lag 0 h and  $\sim \pm 5$  h, respectively. (C) “Memory-loss” flow-cell experiments, where we harvest WT bacteria from FC1 at  $T = \sim 30$ –40 h and maintain them in culture tubes for different time intervals ( $t_r = 0$  h, 14 h, and 37 h) before introducing them to FC2. Solid lines represent data of number of surface bacteria per frame vs. time. Dashed lines represent data fit to exponential functions. Shaded areas represent 95% CI of the fits.  $t_{\text{lag}}(t_r = 0 \text{ h}) = 4.68 \text{ h}$  [4.65 h, 4.72 h],  $t_{\text{lag}}(t_r = 14 \text{ h}) = 5.46 \text{ h}$  [5.44 h, 5.48 h], and  $t_{\text{lag}}(t_r = 37 \text{ h}) = 13.41 \text{ h}$  [13.39 h, 13.42 h]. Near-complete “memory loss” occurs by  $t_r = 37$  h.

maximal cAMP levels, and maximal cAMP levels occur  $\sim 5$  h after maximal TFP activity. This  $\sim 5$ -h offset is clearly longer than an average single division time ( $\sim 1$  h, Fig. S1); thus, cAMP-TFP correlations are inherently multigenerational. In fact, cAMP and TFP activity are anticorrelated at time lag = 0 h (Fig. 4B, *Right*). Additional family correlation data are shown in Fig. S10. These effects lead to damped but coupled multigenerational oscillations of TFP activity and cAMP, and the cross-correlation peak value of  $\sim 5$  h agrees well with previous observed time scales for reaching peak TFP-dependent cAMP levels after surface engagement (8).

A key aspect of this model is its predictive value. The values of exponential decay parameters  $k$  and  $k_s$  extracted from fits to cAMP-TFP data indicate that the oscillations are strongly damped and suggest that surface engagement should have a composite decay time on the order of  $\sim 10$  h. That is, surface-engaged cells (WT in FC2) should return to planktonic-like behaviors (WT in FC1) within several decay periods after the cells have been removed from the surface environment. WT bacteria are harvested from FC1 at a higher surface cell density ( $T = \sim 30$ –40 h), maintained in culture tubes as planktonic cells (using the same growth conditions as the overnight planktonic growth before inoculation)

for different time intervals ( $t_r = 0$  h, 14 h, and 37 h), and then regrown to exponential phase for  $\sim 3$  h before introducing these planktonic populations to a new FC2 (Fig. 4C and *SI Materials and Methods*). We hypothesize that as the time interval away from the surface increases (i.e., longer periods of unperturbed planktonic growth), the damped cAMP–TFP oscillations will dissipate and harvested cells will “lose memory” of the surface. Consistent with this hypothesis, we find progressive decrease of attachment with increasing  $t_r$ . In fact, cells with a  $t_r = 37$  h (i.e., 37 h of overnight planktonic growth in a culture tube) show little evidence of the enhanced surface attachment associated with surface-sentient cells ( $t_{lag} = 13.41$  h), similar to the WT in FC1 in Fig. 1B, Top ( $t_{lag} = 17.56$  h). These findings are consistent with just under four decay times ( $\sim 4 \times 10$  h) for a loss of surface memory, in surprisingly good agreement with our simple model. Moreover, the loss of memory is “dose-dependent” on the period of planktonic incubation. Shorter periods of planktonic incubation show a time-dependent shorter  $t_{lag}$  until exponential increase of surface colonization is restored (Fig. 4C).

**cAMP–TFP Correlations Result in Collective Suppression of TFP Motility for Entire Lineages Rather than Single Cells.** To assess differences in coordination of TFP activity and cAMP levels between cells that make low-generation, one-legged family trees in FC1 and cells that make high-generation, two-legged family trees in FC2, we examined the intracellular cAMP levels and TFP activity (measured by the fraction of time with detectable TFP twitching activity) in Fig. 5A from 31 bacteria families in FC1 (Left) and five families in FC2 (Right). Fig. 5A, Left shows that cAMP and TFP activity are uncorrelated for cells at early stages of surface sensing in FC1 (Spearman correlation:  $\rho = -0.153, P = 0.29$ ). This observation can be contrasted with the behavior of cell lineages in FC2, which are composed mainly of previously surface-engaged bacteria (Fig. 5A, Right). Intracellular cAMP levels are strongly anticorrelated with TFP activity at time lag = 0 h in FC2 (Spearman correlation:  $\rho = -0.643, P = 4.69 \times 10^{-7}$ ), in agreement with both the experimental and calculated cAMP–TFP correlations at time lag = 0 h in Fig. 4. In fact, cells in FC2 from different lineages fall on the same curve, consistent with the expectation that they use the same mechanism of surface sensing. These results imply that the emergence of correlations between cAMP and TFP are related to the architecture of resultant family trees, which control surface population growth.

We investigated how the development of correlations between cAMP and TFP influence individual cell TFP-mediated motility. We observed an unanticipated state intermediate between planktonic and sessile existence, one in which suppression of TFP motility is enforced across an entire lineage of cells via cAMP–TFP multigenerational memory. Importantly, the lineage-scale TFP motility coordination strongly impacts the number of surface-adhered cells with near-zero TFP motility. Fig. 5B compares histograms depicting the intensity of TFP activity for family trees in FC1 (Left) and FC2 (Right). At early stages of attachment (FC1), we observe a roughly uniform distribution of TFP activity for all cells. At later stages of incubation (FC2), an approximately threefold increase in the bin with near-zero TFP motility is observed. Comparing the distributions between FC1 and FC2 in Fig. 5B using a Kruskal–Wallis test yields a  $P$  value  $\ll 10^{-5}$ . The occurrence of this intermediate state correlates with the appearance of large multigenerational family trees that lead to exponential population increases in FC2.

## Discussion

We observe strong differences in surface attachment behavior between surface-naïve and surface-sentient cells. Surface cells in FC2 exhibit a subpopulation with higher cAMP levels than those in FC1, organize into family trees with more generations than those in FC1 on average, and increase the surface population drastically immediately after exposure rather than exhibiting a long  $\sim 20$ -h lag phase as observed for cells in FC1. This lag phase is a direct consequence of the surface-sensing process. We show

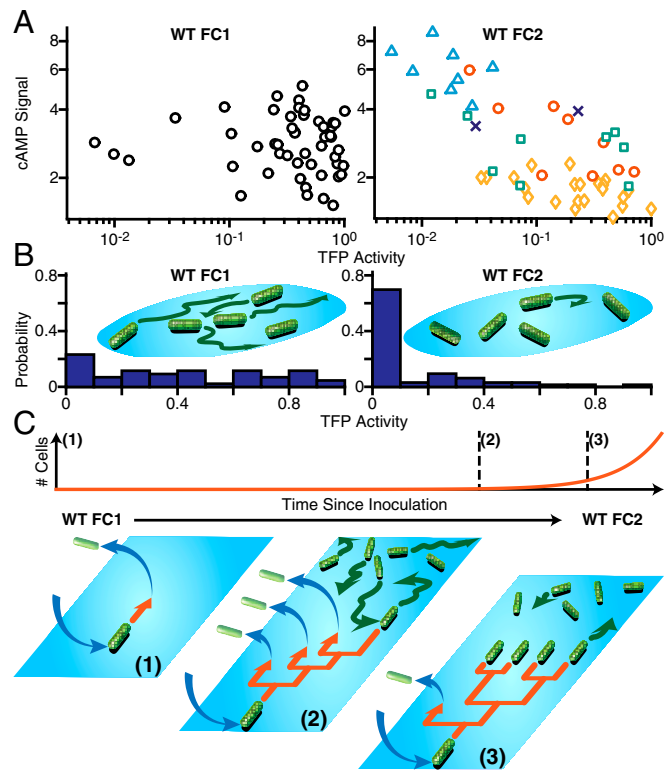


**Fig. 5.** Surface-sentient state involves cAMP–TFP correlations and suppression of TFP motility. (A) Plot of time-averaged (time lag 0 h) cAMP signal vs. TFP activity per bacterium for 50 bacteria in 31 families in WT FC1 (Left) and 95 bacteria in five families in WT FC2 (Right) ( $T = 29.5$  h). For FC1, one symbol is used for individual bacteria. For FC2, each symbol and color represents one family, and each data point is one bacterium in that family. These two quantities are uncorrelated in FC1 (Spearman correlation:  $\rho = -0.153, P = 0.29$ ) and anticorrelated in FC2 (Spearman correlation:  $\rho = -0.643, P = 4.69 \times 10^{-7}$ ). (B) Distributions of time-averaged TFP activity for bacteria that do not detach from the surface. FC2 is statistically different (Kruskal–Wallis test  $P$  value  $\ll 10^{-5}$ ) with approximately threefold more cells having near-zero TFP motility. (C) Model for different stages of early biofilm growth. Stage (1): When engaging a virgin surface, essentially all attaching cells detach almost immediately and do not stay long enough to divide (Bottom). The surface population is near-zero (Top). Stage (2): Cells begin to stay on the surface for more than a generation with increased cAMP and TFP activity, but typically with one-legged division branching (Bottom). The surface cell population increases from zero to a low value, since one-legged trees do not significantly increase the population (Top). Stage (3): cAMP and TFP activity correlate into coupled oscillations, resulting in a new state characterized by suppression of TFP-mediated motility and an increasing number of cells with near-zero TFP activity. These events mediate the emergence of an exponentially increasing population of biofilm bacteria (Top), made possible by the new two-legged family tree architecture (Bottom).

via a Turing model that the idea of a perishable memory is consistent with the Pil-Chp surface-sensing framework.

Although cAMP–TFP correlations can last several generations, we stress that we do not claim that the same single cells that encounter the surface can remember the surface  $\sim 20$  h later. Rather, our observations raise the possibility that surface-sentient cells that detach can retain a memory of the surface imprinted via cAMP, and that the results in FC1 are generated by a changing heterogeneous planktonic population that starts out predominately surface-naïve but is progressively enriched by a surface-sentient subpopulation via cells that have previously landed on the surface. This process results in a planktonic population with varying degrees of surface adaptation, which can render the apparent memory of a population quite long.

These observations imply that the transition from planktonic to biofilm phenotype in *P. aeruginosa* PA14 does not proceed via

the common assumption that cells stay on the surface progressively longer as they “sense” the surface. Reversible attachment is a structural part of irreversible attachment. The repeated cycle of sensing, division, and detachment creates a planktonic population with a robust cAMP–TFP-based memory of the surface, allowing cells to return to the surface progressively better adapted for sensing and attachment.

Results here suggest that we can better define the historical classifications of “reversible” and “irreversible” attachment in biofilm formation (Fig. 5C). There is an initial period where essentially all attaching cells detach almost immediately, followed by a period during which attaching cells stay long enough to divide, but almost all subsequent divisions result in one daughter cell’s detaching (one-legged family trees). Analysis of correlations between cAMP levels and TFP activity for cells in such family trees shows that these quantities are uncorrelated at this early stage. Moreover, we note that cells during these two initial stages spend a large fraction of time in the vertical orientation perpendicular to the surface. We propose that these initial periods roughly correspond to “reversible” attachment, before cells have committed to the surface. With the onset of surface sensing, intracellular cAMP levels and TFP activity for cells in a given lineage become correlated into damped coupled oscillations, which subjects that lineage to repeated suppression of TFP-mediated motility, resulting in a sharp increase in the number of cells with near-zero TFP motility. (That these cells eventually become sessile with no TFP activity is consistent with the trend of dissipating cAMP–TFP oscillations.) Since the detachment sequence of *P. aeruginosa* involves both TFP and flagellum activity (8), such a reduction in TFP motility can drastically suppress cell detachment (18, 23) and cause the foundational emergence of family tree architectures with predominately two-legged division branching (i.e., both daughter cells remain surface-attached), resulting in cells whose progeny dominate the surface population via exponential surface population growth. We suggest that this motility-suppressed state can be used to define the onset of “irreversible attachment.” Therefore, not only does multigenerational surface sensing allow planktonic cells to “remember” a surface, it directly leads to a form of surface commitment defined in terms of cooperative behavior in a lineage of cells rather than in terms of single-cell behavior.

1. Liu J, et al. (2015) Metabolic co-dependence gives rise to collective oscillations within biofilms. *Nature* 523:550–554.
2. Humphries J, et al. (2017) Species-independent attraction to biofilms through electrical signaling. *Cell* 168:200–209.e12.
3. Liu J, et al. (2017) Coupling between distant biofilms and emergence of nutrient time-sharing. *Science* 356:638–642.
4. Miller MB, Skorupski K, Lenz DH, Taylor RK, Bassler BL (2002) Parallel quorum sensing systems converge to regulate virulence in *Vibrio cholerae*. *Cell* 110:303–314.
5. Davies DG, et al. (1998) The involvement of cell-to-cell signals in the development of a bacterial biofilm. *Science* 280:295–298.
6. Nealson KH, Platt T, Hastings JW (1970) Cellular control of the synthesis and activity of the bacterial luminescent system. *J Bacteriol* 104:313–322.
7. O’Toole GA, Wong GC (2016) Sensational biofilms: Surface sensing in bacteria. *Curr Opin Microbiol* 30:139–146.
8. Luo Y, et al. (2015) A hierarchical cascade of second messengers regulates *Pseudomonas aeruginosa* surface behaviors. *MBio* 6:1–11.
9. Persat A, Inclan YF, Engel JN, Stone HA, Gitai Z (2015) Type IV pili mechanochemically regulate virulence factors in *Pseudomonas aeruginosa*. *Proc Natl Acad Sci USA* 112:7563–7568.
10. Ellison CK, et al. (2017) Obstruction of pilus retraction stimulates bacterial surface sensing. *Science* 358:535–538.
11. Hug I, Deshpande S, Sprecher KS, Pfohl T, Jenal U (2017) Second messenger-mediated tactile response by a bacterial rotary motor. *Science* 358:531–534.
12. Burrows LL (2012) *Pseudomonas aeruginosa* twitching motility: Type IV pili in action. *Annu Rev Microbiol* 66:493–520.
13. Leighton TL, Buensuceso RNC, Howell PL, Burrows LL (2015) Biogenesis of *Pseudomonas aeruginosa* type IV pili and regulation of their function. *Environ Microbiol* 17:4148–4163.
14. Kuchma SL, et al. (2010) Cyclic-di-GMP-mediated repression of swarming motility by *Pseudomonas aeruginosa*: The *pilY1* gene and its impact on surface-associated behaviors. *J Bacteriol* 192:2950–2964.

## Materials and Methods

*P. aeruginosa* PA14 strains WT and  $\Delta pilA$  (14),  $\Delta pilT$ ,  $\Delta pilU$  (16), and  $\Delta pilU$  mutants were used. For cAMP reporter experiments, WT and  $\Delta pilU$  with the YFP/CFP reporter/control plasmid were used (9). M63 supplemented with 1 mM MgSO<sub>4</sub>, 0.05% glucose, and 0.125% casamino acids (CAA) was used for flow cell experiments conducted at 30 °C with a flow rate of 3 mL/h. Flow cells for single-channel and memory-loss experiments were described previously (20, 24). The flow was stopped for bacterial inoculation and 10 min of incubation, and then resumed with recording. For tandem flow cell experiments, flow cell channels were joined in series by connecting the outlet of FC1 with the inlet of FC2.

Images were recorded with an Olympus microscope and an Andor electron-multiplying CCD (EMCCD) camera. Bright-field images were recorded every 3 s, fluorescence every 15 min. Total recording time varied from 10~40 h, which resulted in 12,000~48,000 bright-field images and 40~160 fluorescence images, containing ~1 million bacteria images. The image size was 67 × 67  $\mu\text{m}^2$  (1,024 × 1,024 pixels).

The image analysis software is adapted from methods previously described (18–21, 23, 25, 26) and written in MATLAB R2015a (MathWorks). We use a “family tree” data structure where each tree node is a single bacterium. To minimize errors in recognizing and tracking cells in lineages, we manually validated each tracked family (three or more families per strain). Families were chosen by randomly sampling bacteria in the dataset and reconstructing their families. An example video of validated tracking data is shown in Movie S1.

Pil-Chp-cAMP surface sensing (8, 9) is described with a minimal model. Dynamical equations relating these quantities are coupled and nonlinear, but they can be linearized around a fixed point to examine the fluctuations and response, following the spirit of Alan Turing’s work to describe reaction-diffusion systems (22). The system of equations can be solved, and correlation functions can be calculated and used to manually fit the experimental correlation data.

Full materials and methods are found in *SI Materials and Methods*.

**ACKNOWLEDGMENTS.** We thank Z. Gitai and M. Wolfgang for providing plasmids. C.K.L., J.d.A., A.E.B., R.R.B., R.G., G.A.O., and G.C.L.W. are supported by Human Frontiers Science Program Grant RGP0061/2013. G.A.O. is also supported by NIH Grant R37 AI83256, G.C.L.W. by NIH Grant R01AI102584, K.Z. by the Recruitment Program of Global Experts, and R.R.B. by National Science Foundation Grant NSF-DMR-1506625 and support from the National Cancer Institute of the NIH under Physical Sciences Oncology Center Award U54 CA193417.

15. Chiang P, et al. (2008) Functional role of conserved residues in the characteristic secretion NTPase motifs of the *Pseudomonas aeruginosa* type IV pilus motor proteins PilB, PilT and PilU. *Microbiology* 154:114–126.
16. Caiazza NC, O’Toole GA (2004) SadB is required for the transition from reversible to irreversible attachment during biofilm formation by *Pseudomonas aeruginosa* PA14. *J Bacteriol* 186:4476–4485.
17. Benjamini Y, Yekutieli D (2001) The control of the false discovery rate in multiple testing under dependency. *Ann Stat* 29:1165–1188.
18. Conrad JC, et al. (2011) Flagella and pili-mediated near-surface single-cell motility mechanisms in *P. aeruginosa*. *Biophys J* 100:1608–1616.
19. Utada AS, et al. (2014) *Vibrio cholerae* use pili and flagella synergistically to effect motility switching and conditional surface attachment. *Nat Commun* 5:4913.
20. Zhao K, et al. (2013) Pil trails guide exploration and microcolony formation in *Pseudomonas aeruginosa* biofilms. *Nature* 497:388–391.
21. Jin F, Conrad JC, Gibiansky ML, Wong GC (2011) Bacteria use type-IV pili to slingshot on surfaces. *Proc Natl Acad Sci USA* 108:12617–12622.
22. Turing AM (1952) The chemical basis of morphogenesis. *Philos Trans R Soc Lond B Biol Sci* 237:37–72.
23. Gibiansky ML, et al. (2010) Bacteria use type IV pili to walk upright and detach from surfaces. *Science* 330:197.
24. Tolker-Nielsen T, Sternberg C (2005) Growing and analyzing biofilms in flow chambers. *Current Protocols in Microbiology* (Wiley, New York).
25. Lee CK, et al. (2016) Evolution of cell size homeostasis and growth rate diversity during initial surface colonization of *Shewanella oneidensis*. *ACS Nano* 10: 9183–9192.
26. de Anda J, et al. (2017) High-speed “4D” computational microscopy of bacterial surface motility. *ACS Nano* 11:9340–9351.
27. Brun YV, Marczyński G, Shapiro L (1994) The expression of asymmetry during *Caulobacter* cell differentiation. *Annu Rev Biochem* 63:419–450.